CHEMISTRY
AN ASIAN JOURNAL

DOI: 10.1002/asia.200800331

Iron and Ruthenium Nanoparticles in Carbon Prepared by Thermolysis of Buckymetallocenes

Takahiro Nakae,[a] Yutaka Matsuo,*[a] Masatoshi Takagi,[b] Yuta Sato,[c] Kazu Suenaga,[a, c] and Eiichi Nakamura*[a]

Abstract: Thermolysis of fullerene iron and ruthenium complexes (buckymetallocene $M(C_{60}R_5)Cp$ (M = Fe; R = Ph (**1**) and Me (**2**), M = Ru; R = Ph (**3**), Me (**4**)) under a nitrogen atmosphere produced metal nanoparticles dispersed in carbon materials. The thermal degradation processes of the buckymetallocenes were studied by TG-DTA, TEM with a heating sample stage, and VT-XRD. Variation of the thermolysis temperature led to a change in the size of the nanoparticles and the morphology of the carbon materials. Thermolysis of buckyferrocene at 700 °C gave highly dispersed iron nanoparticles (average diameter of 7.4 nm). After thermal treatment at 900 °C, graphite structures such as carbon nanocapsules and carbon nanotubes formed because of the catalytic activity of the iron nanoparticles. Ruthenium nanoparticles prepared from buckyruthenocene were much smaller than the iron counterparts, and did not catalyze the formation of graphite structures. When buckyruthenocene absorbed on silica gel was heated at 500 °C under a hydrogen atmosphere, the resulting ruthenium nanoparticles showed high activity in catalytic hydrogenation.

Keywords: carbon · fullerenes · iron · nanoparticles · ruthenium

Introduction

Metal nanoparticles have received much attention in materials science because of their potential applications including electromagnetic devices and catalysis.[1–6] These materials have been prepared by reduction of metal salts in micelles or thin films,[7] by a solution process involving the thermal decomposition of organometallic molecular precursors,[8] hydrothermal synthesis,[9] sonication,[10] and pyrolysis of metal-containing polymer.[11] Composites of metal nanoparticles dispersed in carbon matrices have been widely studied as electronic and magnetic materials, and as catalysts for organic synthesis.[12–14] Carbon materials are important solid supports, which are used for immobilization of metal nanoparticles on activated carbons,[13a] carbon nanofibers,[15,16] and carbon nanotubes.[16–19] Fullerene has also been used as a metal-support material.[17,20]

We report here that thermolysis of buckymetallocene compounds $Fe(C_{60}R_5)Cp$ (R = Ph (**1**), Me (**2**)) and $Ru(C_{60}R_5)Cp$ (R = Ph (**3**), Me (**4**)) under an inert atmosphere at 500–700 °C provides a new method for the preparation of iron and ruthenium nanoparticles dispersed in carbon. An attractive feature of this methodology is the possible extension to various other metals, because of the ready availability of a number of stable metal η^5-fullerene complexes $M(C_{60}R_5)Ln$[21,22] from penta(organo)[60]fullerenes $C_{60}R_5H$.[23] These complexes are often stable in air even at high temperature (ca. 300 °C),[22b,h,24] because of the stability of the η^5-coordination. Unique and attractive features of these complexes are that the metal atoms in the starting materials are embedded uniformly in the crystals of bulky fullerene molecules (one metal atom per 1.3 nm^3, estimated from crystal structure data), and that the carbon matrices formed by thermolysis are not contaminated by chalcogenide or metal

[a] Dr. T. Nakae, Dr. Y. Matsuo, Dr. K. Suenaga, Prof. Dr. E. Nakamura
Nakamura Functional Carbon Cluster Project, ERATO
Japan Science and Technology Agency
7-3-1 Hongo, Bunkyo-ku, Tokyo, 113-0033 (Japan)
Fax: (+81) 3-5800-6889
E-mail: matsuo@chem.s.u-tokyo.ac.jp
nakamura@chem.s.u-tokyo.ac.jp

[b] M. Takagi
Mitsubishi Chemical Group Science and Technology Research Center, Inc.
1000, Kamoshida-cho Aoba-ku, Yokohama 227-8502 (Japan)

[c] Dr. Y. Sato, Dr. K. Suenaga
Nanotube Research Center
National Institute of Advanced Industrial Science and Technology (AIST)
Tsukuba 305-8565 (Japan)

Supporting information for this article is available on the WWW under http://dx.doi.org/10.1002/asia.200800331.

pnictogenide atoms,[11b] because the $C_{60}R_5$ ligand contains only carbon and hydrogen atoms.

Thermolysis of the metal complexes will initially generate single metal atoms and organofullerene radicals that will form a fullerene matrix in the thermolysis product.[25] The single metal atoms may move through the fullerene matrix and form small metal clusters, which will then aggregate together to form larger clusters. Such clusters may exhibit their own characteristic properties as they grow larger in the carbon matrices. Thermolysis of buckymetallocene compounds **1–4** under an inert atmosphere at 500–700 °C produced metal nanoparticles dispersed in carbon materials (Scheme 1), which were characterized by transmission electron microscopy (TEM) and X-ray powder diffraction (XRD) observations.

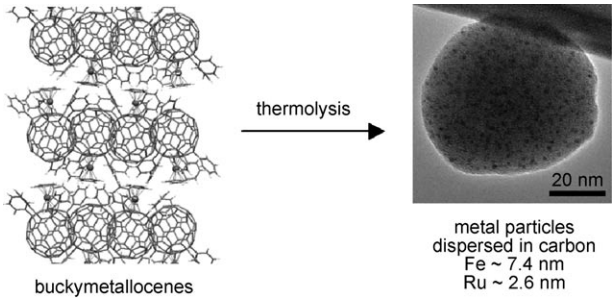

Scheme 1. Preparation of metal nanoparticles from buckymetallocenes.

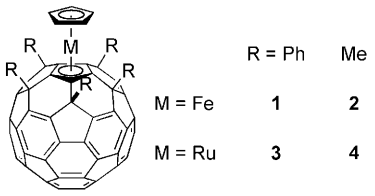

Abstract in Japanese:
フラーレン鉄およびルテニウム錯体(バッキーメタロセン M($C_{60}R_5$)Cp (M = Fe; R = Ph (**1**), Me (**2**), M = Ru; R = Ph (**3**), Me(**4**))の熱分解を窒素雰囲気下で行うことで金属ナノ粒子が分散した炭素材料を得た．バッキーメタロセンの熱分解過程を TG-DTA, 昇温ステージを用いた TEM 観察,および温度可変 XRD 測定を用いて調査した．熱分解温度を変化させることで，ナノ粒子のサイズと炭素材料の形態が変化した．バッキーフェロセンを 700 °C で熱分解することで，高度に分散した鉄ナノ粒子(平均 7.4 nm)が得られた．900 °C での熱処理後，カーボンナノカプセルやカーボンナノチューブといったグラファイト構造が鉄ナノ粒子の触媒作用により形成した．バッキールテノセンより調製したルテニウムナノ粒子は，鉄ナノ粒子よりも小さなサイズになり，グラファイト構造の形成を触媒しなかった．バッキールテノセン担持シリカゲルを水素雰囲気下 500 °C で熱処理を行うことで得られるルテニウムナノ粒子は触媒的水素化反応に高い触媒活性を示した．

Results and Discussion

Bulk Thermolysis of Buckyferrocene (1)

The crystals of buckyferrocene Fe($C_{60}Ph_5$)Cp (**1**)[26] (50.0 mg in a small quartz pan placed in a quartz tube in an electric furnace, Figure S1 of the Supporting Information) were heated from room temperature to 500 °C at a rate of 10 °C min^{-1} under a flow of nitrogen (0.1 L min^{-1}). When the temperature reached 500 °C, the apparatus was cooled to ambient temperature while maintaining the nitrogen flow. A reddish oil was found in the glass wool plugged at the outlet of the tube; a fine brown powder sublimed during the thermolysis and formed a thin film on the inner wall of the quartz tube, and a black carbonaceous solid remained in the quartz pan.

The oily material was extracted with diethyl ether, and an orange solid (8.5 mg) was obtained. GC-MS analysis of the collected materials indicated that the oil contains *m*/*z* 142 (cyclopentadienylbenzene), 154 (biphenyl), and 262 (phenylferrocene) [Eq. (1), Chart S1 of the Supporting Information]. The phenyl group must have come from the $C_{60}Ph_5$ moiety and the cyclopentadienyl group from the ferrocene moiety. One can speculate that these products are the results of either pure radical or iron-catalyzed reactions. A hypothetical reaction pathway is shown in Equation (2), where radical species are shown for simplicity. In the light of the extensive iron-catalyzed C–C bond reorganization observed at higher temperature (e.g., graphene and nanotube formation, vide infra), the iron-catalyzed decomposition is also likely. The solid material on the inner wall of the quartz tube was washed out with toluene to obtain a black solid (0.7 mg). HPLC indicated that it is [60]fullerene (Chart S2 of the Supporting Information). Fullerene is known to sublime at high temperatures.[27] Note that heating a mixture of [60]fullerene and ferrocene instead of the buckyferrocene under nitrogen resulted in sublimation of both compounds rather than chemical reactions. To prove the advantage of using a buckyferrocene as opposed to a mixture of ferrocene and fullerene, we also performed the TG-DTA analysis of the ferrocene/fullerene cocrystal, $C_{60}(C_{10}H_{10}Fe)_2$[28] (Figure S2 if the Supporting Information). As one might expect, ferrocene started sublime at low temperature, followed by the sublimation of fullerene. All materials sublimed during the analysis, and no metal nanoparticle–carbon composite remained. This result provides strong support of the advantageous use of buckymetallocenes for the preparation of metal nanoparticles embedded in carbon materials.

The carbonaceous residue in the pan was dispersed in methanol and weighed 35.0 mg after drying. Subsequent toluene extraction of the material indicated that it contained no free [60]fullerene. Elemental analysis indicated an ele-

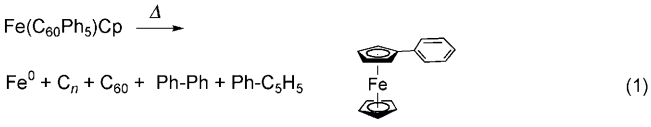

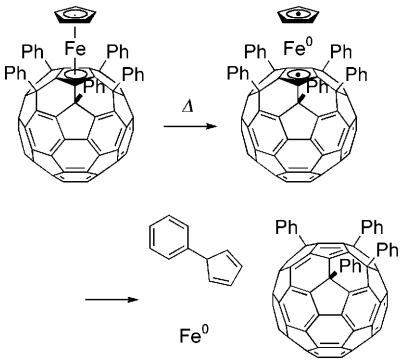

(2)

mental composition of C 92.5%, H 1.3%, N 0%, and we assigned the remaining 6.2% to the iron content. It is important to know how much of the 6.2% iron content is exposed on the surface of the carbon. Thus, we extracted the surface iron from the carbonaceous reside (5.00 mg) into hydrochloric acid, and determined the iron content by absorptiometric analysis (2,4,6-tris(2-pyridyl)triazine as an indicator). This analysis indicated that 2.6×10^{-2} mg of iron and hence, approximately 8% of all iron content is exposed on the surface.

The XRD data of the carbonaceous residue (Figure S3 of the Supporting Information) is similar to the VT-XRD data at 600°C (Figure 5) except that the α-Fe peak (JCPDS card No. 06-0696) was absent, indicating that the nanoparticles are extremely small. Further studies indicated that the particle size can be controlled by changing the thermolysis temperature. In the following paragraphs, we describe the nature of the particle formation process and the properties of the material as studied by TG-DTA, TEM with a heating sample stage, and VT-XRD.

Thermogravimetric Analysis for Buckyferrocenes 1 and 2

We first carried out thermogravimetry-differential thermal analysis (TG-DTA) of the crystals of buckyferrocene Fe($C_{60}Ph_5$)Cp (**1**)[26] under a flow of nitrogen (Figure 1). The buckyferrocene **1** decomposed in four consecutive steps. Heating in the 100–400°C temperature range resulted in the loss of 6 wt% of material. The mass loss at lower temperature can be ascribed to the loss of water or small amount of the solvent molecules (benzonitrile and CS_2 that are used in the synthesis and reprecipitation) included in the powdery sample. A 16 wt% loss occurred in the temperature range from 400 to 570°C, which can be ascribed to the loss of the phenyl groups and the cyclopentadienyl iron group from the fullerene core. There also occurred sublimation of a small amount of [60]fullerene (vide supra). We believe that the loss of the organic and inorganic groups generated some reactive species and caused cross-linking of the fullerene molecules.[25,27] In addition, single atomic divalent iron atoms must have been released from the coordination sphere of the fullerene molecule and transformed to zero-valence iron, as supported by the formation of α-Fe metal particles observed in the XRD analysis (vide infra). An exothermic event that did not affect the weight loss profile was observed at 840°C. Combined with the analysis shown below, the exothermic reaction at 840°C is probably iron-catalyzed conversion of the carbon matrix derived from fullerene into graphitic structures. TG-DTA of the crystals of a pentamethylated buckyferrocene Fe($C_{60}Me_5$)Cp (**2**)[22b] showed a behavior similar to that of the pentaphenyl compound **1** (Figure S4 of the Supporting Information).

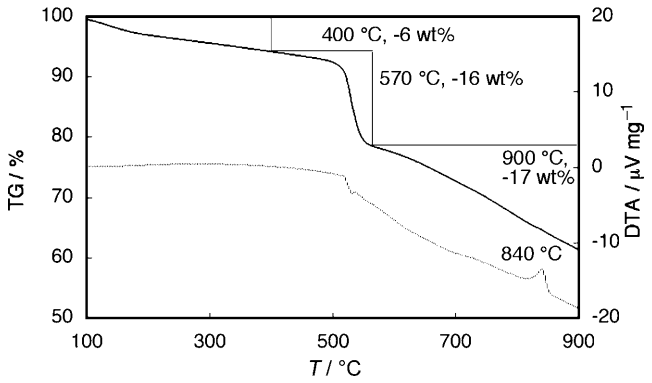

Figure 1. TG-DTA curve of Fe($C_{60}Ph_5$)Cp (**1**) at a rate of 10°C min^{-1} a under flow of nitrogen (0.10 L min^{-1}). The solid line and the dotted line are TG and DTA data, respectively.

TEM Observation of Carbonaceous Materials from the Buckyferrocene

The product obtained in the above TG-DTA experiments for Fe($C_{60}Me_5$)Cp (**2**) was ground into powder, and subjected to TEM observation. The TEM images are shown in Figure 2 and S4–S12 of the Supporting Information. The materials produced upon heating to 700°C on a TG-DTA in-

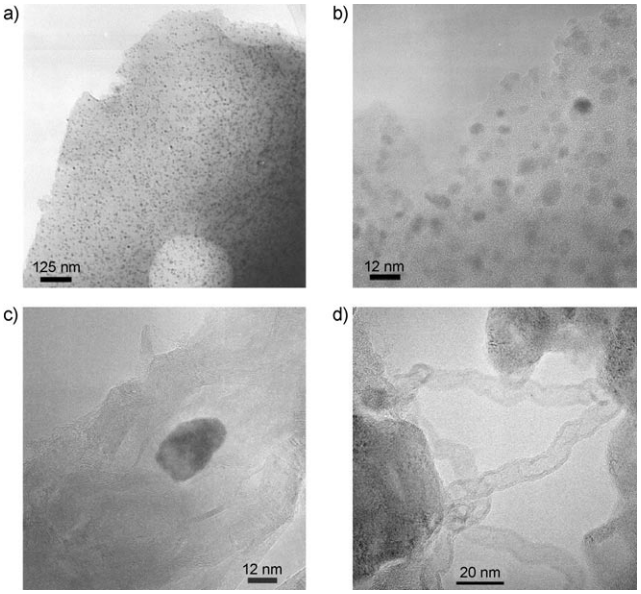

Figure 2. TEM observation of carbonaceous materials obtained by controlled thermolysis of Fe($C_{60}Me_5$)Cp (**2**) in the TG-DTA instrument. (a and b) 700°C, (c and d) 900°C. For larger pictures of the same images, see the Supporting Information.

strument (Figures 2a and b, and S5 and S6 of the Supporting Information) contained iron nanoparticles dispersed in a carbon matrix with an average diameter of 7.4 nm (standard deviation 1.6 nm, Figure 3a). We did not observe any defined carbon structures (e.g., graphene, [60]fullerene crys-

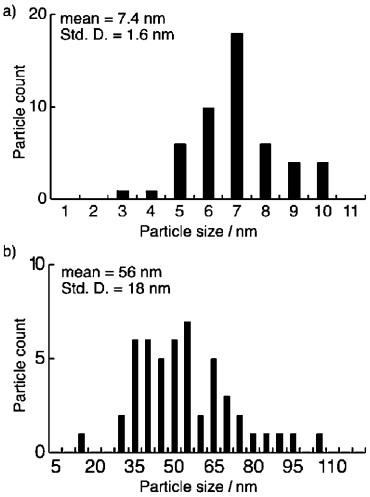

Figure 3. Particle size histogram of iron nanoparticles obtained by TG-DTA analysis of $Fe(C_{60}Me_5)Cp$ (**2**) a) to 700 °C, b) to 900 °C.

tals, crystals of the starting material). As discussed further in the thermal analysis section, graphitization of the carbon matrix took place during the thermolysis to 900 °C. TEM images of the resulting samples obtained under these conditions are shown in Figures 2c and d, and S6–S12 of the Supporting Information. The size of the iron particles was found to be much larger, ranging from 20 nm to 100 nm with an average diameter of 56 nm (standard deviation 18 nm, Figure 3b, TEM images: Figure S7 and S8 of the Supporting Information). We also observed distinct graphitic structures (Figure S9 of the Supporting Information), such as a nanocapsule structure containing an iron nanoparticle[29] (Figure 2c, and S10 and S11 of the Supporting Information) and multi-wall carbon nanotubes (Figure 2d, and S12 and S13 of the Supporting Information). The presence of sulfur contamination (even at low levels, as Fe/S = 500:1) may have an effect on graphitization and nanotube formation.[30] However, we believe that there is practically no remaining CS_2 molecule in the powdery sample after the gradual heating to 500 °C to decompose the buckyferrocene. The formation of these graphitic structures suggests that the iron nanoparticles migrated through the carbon matrix and catalyzed C–C bond reorganization.[31] It is clear that the thermolysis released single iron atoms from the fullerene core in **1** with expulsion of organic groups [Eq. (1) and (2)], causing them to migrate through the carbon matrix to gradually form small nanoparticles at 500–700 °C, which then caused the formation of iron particles, carbon nanotubes, and carbon nanocapsules at 800–900 °C, at which temperature the particle size has grown to be bigger than at 700 °C.

Direct TEM Observation of Thermolysis of Buckyferrocene on a Heating Sample Stage

To connect the bulk experiments, TG-DTA, and TEM results together, we next performed in situ TEM observations of the process of thermolysis of the buckyferrocene with the aid of a TEM instrument equipped with a variable temperature stage. We chose the pentamethyl compound **2** to avoid contamination of the TEM column by high molecular weight organometallic fragments during heating in vacuum. Particles of compound **2** that are several tens of nanometers in diameter (see Figure 4) were observed on a heating

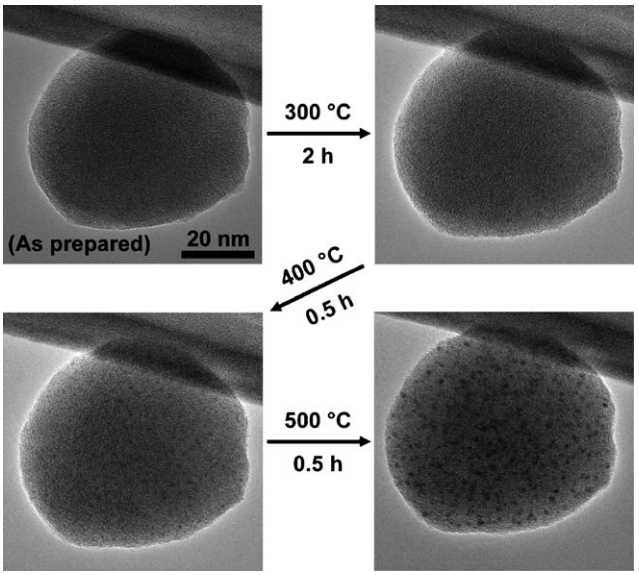

Figure 4. TEM analysis of $Fe(C_{60}Me_5)Cp$ (**2**) with a heating sample stage at an accelerating voltage of 120 kV.

sample stage under the TEM conditions. No change was apparent after heating the sample at 300 °C for 2 h, and small iron nanoparticles of about 1.4 nm diameter appeared after heating for 0.5 h at 400 °C. Iron particles grew larger to 2.8 nm after heating for 0.5 h at 500 °C, indicating that metal atoms and/or metal clusters move in the carbon matrix.[32] Iron nanoparticles grew even larger by aggregation at 500 °C. The outline of the particles remained unchanged during the observation, as is seen in Figure 4. The in situ TEM observations closely paralleled the results of the bulk experiments, except that the iron particles observed at each temperature are slightly smaller. This difference may have arisen from the difference in the substrate (**1** vs **2**) and the 120 kV electron irradiation in high vacuum.

Variable Temperature-XRD Analysis of the Buckyferrocene

To obtain information on the time-dependent change of the structures on the aggregated iron and of the carbon matrix, we carried out variable temperature XRD (VT-XRD) analysis of buckyferrocene **1** under a flow of nitrogen (Figure 5).

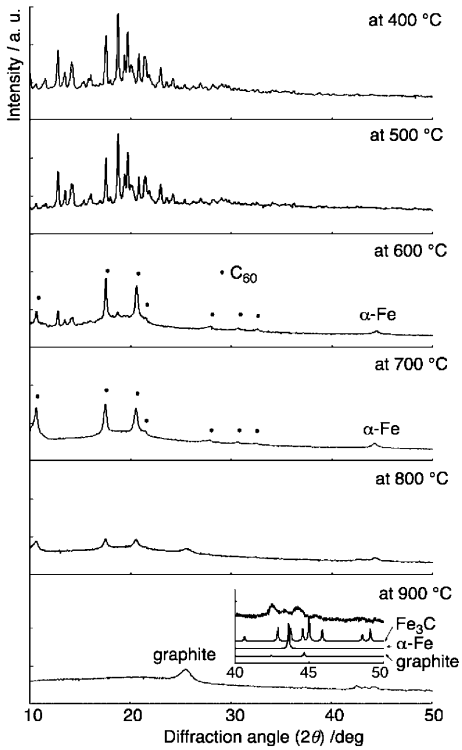

Figure 5. VT-XRD analysis of $Fe(C_{60}Ph_5)Cp$ (**1**) under a flow of nitrogen (0.2 L min^{-1}). The temperature program used a rate of +50 °C min^{-1}, then +2 °C min^{-1} from 10 °C before the measurement temperature, then it held the temperature for 3 min before starting the measurements. Measurement conditions: scan range, 10–70° [2θ]; sampling, 0.02°; scan rate, 1°/min.

At 400 °C, the observed pattern can assign the crystalline morphology of **1**, indicating that the buckyferrocene is stable at this temperature (in agreement with the spectroscopic analysis of the products after heating). At 600 °C, the intensity of the crystal pattern of buckyferrocene decreased, and the crystal pattern of [60]fullerene (JCPDS card No. 47-0787) as well as another peak at $2\theta = 44°$ corresponding to α-Fe (JCPDS card No. 06-0696) appeared. The particle size of the α-Fe particles was estimated as 12 nm, as calculated by Scherrer's equation from the peak width at half height of the iron peak ($D = k\lambda/\beta cos\theta$ where k is a constant equal to 0.9, λ is the X-ray wavelength equal to 0.154 nm, β is the width at half maximum, and θ is the half diffraction angle). The particle size distribution of this sample is larger than that of the sample obtained after TG-DTA observed under TEM. This is probably as a result of the much longer heating time for the VT-XRD analysis, which requires 60 min for each scan. At 700 °C, we find patterns resulting from [60]fullerene and α-Fe. The iron particles have grown further to have an average diameter of 20 nm. Upon further heating to 900 °C, the diffraction peaks corresponding to [60]fullerene diminished and another new peak $2\theta = 26°$ arising from the graphite structure (JCPDS card No. 26-1079) was observed. The diffraction peak corresponding to the iron components around $2\theta = 44°$ now shows a complicated pattern, which can be ascribed to the presence of both α-Fe and cementite (Fe_3C, JCPDS card No. 35-0772; Figure 5, inset).[33] The formation of cementite can be explained using the iron–carbon binary phase diagram.[34] The XRD data at 900 °C is in good agreement with the TEM images of the TG-DTA sample obtained after heating to 900 °C (Figure 2c, d), in which we observed nanocapsule and nanotube formation.

Thermogravimetric Analysis of Buckyruthenocene

Considering that the melting point of ruthenium metal is higher than that of iron (Ru, 2334 °C and Fe, 1535 °C) and the high Tamman temperature (T_{Tamman}, 1089 °C for ruthenium) at which sintering occurs,[32] we expected that the ruthenium nanoparticles obtained by thermolysis of buckyruthenocene would be smaller in size than the iron particles from buckyferrocene, and this was indeed the case. We first studied the thermal behavior of buckyruthenocene by TG-DTA. A crystalline powder of buckyruthenocene $Ru(C_{60}Ph_5)Cp$ (**3**)[35] was heated under a flow of nitrogen between a temperature range of 100 to 900 °C with a heating rate of +10 °C min^{-1} (Figure 6). The weight loss of the buckyruthenocene **3** found in the temperature range from 500 to 650 °C (−10 wt %) is much smaller than the corresponding buckyferrocene **1** (−16 wt %, Figure 1), which may suggest a weaker C–C bond cleavage and C–C bond formation ability of the ruthenium nanocluster than that of the iron nanocluster. Unlike the DTA data for the buckyferrocene **1**, which showed an exothermic peak at 840 °C, the DTA data for the buckyruthenocene showed no sign of such an exothermic peak, suggesting that ruthenium nanoparticles do not catalyze graphitization. This is further verified by the TEM analysis reported later. TG-DTA data of the crystalline solids of pentamethyl buckyruthenocene $Ru(C_{60}Me_5)Cp$ (**4**)[22g] showed a distinct weight loss process corresponding to solvent loss around 120 °C, the following thermal decomposition was similar to that of compound **3** (Figure S16 of the Supporting Information).

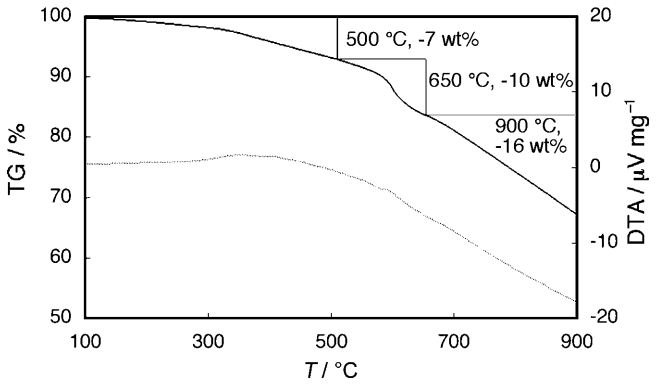

Figure 6. TG-DTA curve of $Ru(C_{60}Ph_5)Cp$ (**3**) at the rate of a 10 °C min^{-1} under a flow of nitrogen (0.10 L min^{-1}). The solid line and the dotted line are TG and DTA data, respectively.

TEM Observation of Carbonaceous Materials from Buckyruthenocene

As reported for buckyferrocenes, we investigated the formation of ruthenium nanoparticles. The TEM images of carbonaceous materials obtained by TG-DTA analysis of **4** at 900 °C (Figure 7, and S17 and S18 of the Supporting Information) showed that ruthenium nanoparticles are finely dispersed in carbon as nanoparticles with an average diameter of 2.6 nm (standard deviation 0.5 nm, Figure 8).

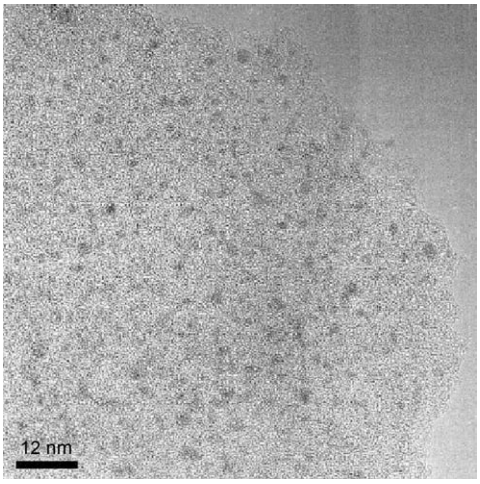

Figure 7. TEM observation of carbonaceous residue from $Ru(C_{60}Me_5)Cp$ (**4**) after thermolysis on the TG-DTA analysis at 900 °C.

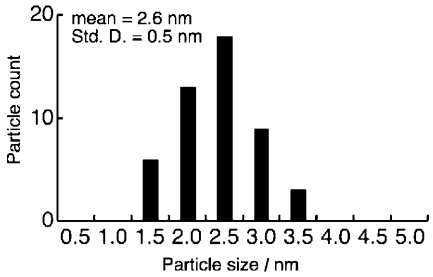

Figure 8. Particle size histogram of ruthenium nanoparticles obtained by TG-DTA analysis of $Ru(C_{60}Me_5)Cp$ (**4**) to 900 °C.

Variable Temperature-XRD Analysis of Buckyruthenocene

The VT-XRD analysis of the buckyruthenocene **3** was carried out under a flow of nitrogen (Figure 9). At 400 °C, a complex diffraction pattern consisting of many peaks was observed, and is identical to the powder pattern simulation based on the X-ray crystal structure of compound **3** without crystal solvent (Figure S15 of the Supporting Information).[36] Upon heating to 700 °C, the pattern of the crystals of **3** disappeared, and a peak at 44° [2θ] corresponding to ruthenium metal (JCPDS card No. 06-0663) appeared. In contrast to the buckyferrocene case, peaks arising from [60]fullerene crystals were not observed. On further heating at 900 °C, peaks corresponding to ruthenium particles (38,

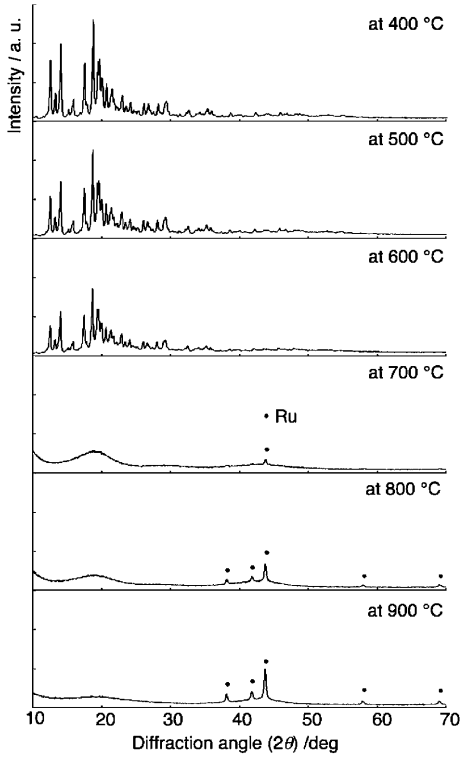

Figure 9. VT-XRD analysis of buckyruthenocene **3** under a flow of nitrogen (0.2 L min^{-1}). The temperature program used a rate of +50 °C min^{-1}, then +2 °C min^{-1} from 10 °C before the measurement temperature, then it held the temperature for 3 min before starting the measurements. Measurement conditions: scan range, 10–70° [2θ]; sampling, 0.02°; scan rate, 1°/min. Each measurement took 60 min.

42, 44, 58, and 69°) became distinct. It is notable that, unlike the buckyferrocene case, there were no graphite peaks at any temperature, which is consistent with the TG-DTA curve (Figure 6) as well as the TEM observation of the thermolysis products in the TG-DTA experiments (Figure 7). We surmise that the ruthenium nanoparticles do not catalyze graphitization of the carbon matrix below 900 °C.

Investigation of the Catalytic Activity of Ruthenium Nanoparticles Dispersed in Carbon Materials

The ruthenium nanoparticles prepared from buckyruthenocene were tested for hydrogenation catalytic activity, and they showed very weak catalytic activity (iron materials prepared from **1** did not show any activity). One might consider that the metal nanoparticles are buried in the carbon substrate rather than exposed on the surface. With the intention of making more active nanoparticles, we examined a solid support approach. Buckyruthenocene **3** was absorbed on silica gel (10 wt %) by impregnation of silica gel in a CS_2 solution of **3**. After evaporation and drying, thermolysis of the buckyruthenocene absorbed on silica gel was carried out under a flow of nitrogen ($Ru–C/SiO_2–N_2$) or under a flow of hydrogen ($Ru–C/SiO_2–H_2$).

Catalytic activities of ruthenium-dispersed materials were investigated for hydrogenation of cyclohexene (Figure S19 of the Supporting Information). Ru–C/SiO_2–N_2 consumed some hydrogen gas but afforded only 2% of hydrogenated product, as analyzed by GC analysis of the reaction mixture after 30 min. On the other hand, Ru–C/SiO_2–H_2 was much more active. Cyclohexene was completely consumed after 3 min. The Ru–C/SiO_2–H_2 catalyst can be reused in the second run without loss of catalytic activity. The large difference in reactivity between Ru–C/SiO_2–H_2 and Ru–C/SiO_2–N_2 may come from different morphologies (i.e., particle size, and so forth).[37] Structure characterization of these complexes is for further work.

The reaction rates of the hydrogenation were compared for Ru–C/SiO_2–H_2 and a commercial Ru–C catalyst (5% Ru, Aldrich) under a hydrogen pressure of 10 bar. In both cases, hydrogen uptake started after an induction period, being longer for Ru–C/SiO_2–H_2. The initial rates were obtained from the slope of the line fitted from 0.3 mmol to 0.7 mmol of hydrogen uptake (Figure 10). The initial rates

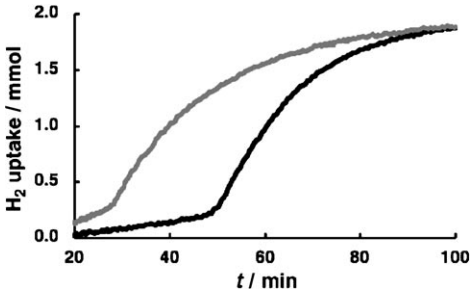

Figure 10. Time course of hydrogen uptake for catalytic hydrogenation of cyclohexene using ruthenium catalysts. The black line and the gray line are Ru–C/SiO_2–H_2 and 5% Ru–C, respectively. Reaction conditions: cyclohexene (2 mmol), ethanol (2 mL), ruthenium catalyst (0.50 mmol), hydrogen (10 bar), 50 °C.

of Ru–C/SiO_2–H_2 and 5% Ru–C were comparable to each other, $1.26(2)\times10^{-6}$ and $1.17(2)\times10^{-6}$ mol s^{-1}, respectively, [Eq. (3)]. We attribute the long induction period to the period required for reduction of the oxidized surface of the metal particles.

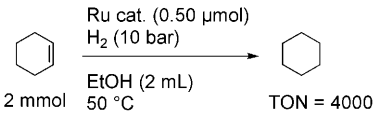

(3)

Catalyst	k [H_2] [mol s^{-1}]	TOF [s^{-1}]
Ru-C/SiO_2-H_2	1.26(2) x 10^{-6}	2.5
5% Ru-C (Ald)	1.17(2) x 10^{-6}	2.3

Conclusions

We have developed a simple method for the preparation of iron and ruthenium nanoparticles finely dispersed in a carbon matrix that is composed almost exclusively of carbon atoms (and a very small fraction of hydrogen atoms). The iron nanoparticles showed good catalytic activity for C–C bond reorganization that results in the formation of carbon nanotubes and capsules, while the ruthenium nanoparticles did not show such an activity. The ruthenium nanoparticles are much smaller in size (ca. 2.6 nm diameter at 900 °C) than the iron particles. This is probably a result of the much higher sintering and melting temperatures of metallic ruthenium. A dominant portion of the iron and ruthenium particles made by the prototype method is buried inside the carbon matrix. For the preparation of nanoparticles with more metal exposed on the surface, thermolysis of metallocene-impregnated silica gel may be a method of choice. Thus, the ruthenium nanoparticles supported on silica show moderate catalytic activity in olefin hydrogenation. On the other hand, protection of easily oxidized elements with a thin shell of non-reactive material such as carbon could be interesting.

The size and morphology of the metal particles can be controlled by the thermolysis conditions (e.g., temperature and the TEM conditions), and perhaps by the use of a silica gel support. We expect that the method can be applied to thermolysis of various other metal η^5-fullerene complexes[21] for controlled preparation of metal nanoparticles on carbon. Being soluble in various solvents and generally stable enough to be sublimed in vacuum,[24] the metal η^5-fullerene complexes can be made into thin films and into micropatterns on various substrates,[38] which may be further converted into carbon-supported metal nanoparticles. One possible application of such films may be their use as a catalyst for carbon nanotube synthesis on a solid support,[39] which will be the subject of further studies. In the light of the availability of bimetallic complexes of deca(organo)[60]fullerenes,[40] we expect that the method will allow the synthesis of heterobimetallic nanosized alloys embedded in carbon matrices. Such mixed-metal systems are interesting materials because of their potential use in memory storage devices and biomedicine.[41]

Experimental Section

General. Thermogravimetry and differential thermal analysis (TG-DTA) were performed on a RIGAKU Thermoplus II TG/DTA instrument. Variable temperature X-ray powder diffraction pattern (VT-XRD) measurements were measured on a RIGAKU RINT-TTR III with Reactor X using $Cu_{K\alpha}$ radiation. X-ray powder diffraction patterns (XRD) were performed on a RIGAKU Minifrex using $Cu_{K\alpha}$ radiation or a RIGAKU R-Axis Rapid II with imaging plate detector using $Cu_{K\alpha}$ radiation. Transmission electron microscopy (TEM) observations were performed using a JEOL 2010F microscope operated at an accelerating voltage of 120 kV with a heating sample stage (JEOL EM-21130). Gas chromatography mass spectrometry (GC-MS) was performed using a Shimadzu GCMS-PAVUM2 equipped with glass capillary column Restek Rtx-5MS

(0.25 mm (i.d.)×30 m). Parameters were as follows: initial temperature, 50 °C; ramp, 10 °C min^{-1}; final temperature, 250 °C; injector-port temperature, 250 °C; detector temperature, 250 °C; injection volume, 1 μL. Analytical HPLC was performed on a Shimadzu HPLC system (column, Cosmosil-Buckyprep, 4.6×250 mm, Nacalai Tesque; flow rate, 2.0 mL min^{-1}; eluent, toluene/2-propanol (7:3); detector, Shimadzu SPD-M10Avp). X-ray fluorescence (XRF) spectrometry was performed for elemental analysis on an SII SEA2120 L.

Materials. Fe($C_{60}R_5$)Cp (R = Ph (**1**), Me (**2**)), and Ru($C_{60}R_5$)Cp (R = Ph (**3**), Me (**4**)) were synthesized according to the previous reports.[22b,g] Powdery samples were prepared with rapid reprecipitation by addition of methanol into CS_2 solutions of the compounds, followed by dryness under vacuum. The obtained powdery materials contain microcrystals, as determined from the XRD measurements. 2,4,6-tris(2-pyridyl)triazine (TPTZ, for iron analysis, Kanto Chemical), hydrochloric acid (for iron analysis, Kanto Chemical), hydroxylamine hydrochloride (TCI), sodium acetate (anhydrous, Wako Chemical), and sodium perchlorate (anhydrous, Kanto Chemical) were used as received. MilliQ-water was used in all experiments. TPTZ aqueous solution (1 M) was prepared by dissolving TPTZ (31.2 mg) in 100 mL of water containing three drops of hydrochloric acid. Aqueous hydroxylamine hydrochloride solution (10 %) was prepared by dissolving hydroxylamine hydrochloride (10 g) in water (90 mL), then purified by adding TPTZ aqueous solution (1 M, 1 mL), sodium perchlorate (1 g) followed by extraction with nitrobenzene (10 mL). Aqueous sodium acetate solution (30 %) was prepared and used without further purification.

TG-DTA analysis. Samples (ca. 5 mg) were transferred in a quartz pan to the instrument under a stream of nitrogen (0.10 L min^{-1}). They were then heated at a rate of 10 °C min^{-1} to the desired temperature. Nitrogen flow (0.10 L min^{-1}) was maintained during the TG-DTA runs.

TEM analysis. Carbonaceous materials were obtained from TG-DTA runs to the desired temperature under a flow of nitrogen. The samples for TEM were prepared by grinding, and dispersion of a large number of particles of carbon material through a slurry in acetone onto a holey carbon film on a Cu grid (300 mesh).

TEM analysis with a heating sample stage. Powdery buckymetallocene samples were sprinkled onto copper TEM grids (150 mesh) coated with holey carbon films. TEM images of the samples were obtained at various temperatures between 298 and 773 K.

VT-XRD analysis. The measurement was performed under a flow of nitrogen (0.20 L min^{-1}). The temperature program used a rate of +50 °C min^{-1}, then +2 °C min^{-1} from 10 °C before the measurement temperature, then the temperature was held constant for 3 min before starting the measurements. Measurement conditions: scan range, 10–70° [2θ]; sampling, 0.02°; scan rate, 1°/min.

Thermolysis of 1. Buckyferrocene **1** (50.0 mg) was placed in a quartz boat inside a quartz tube in a tube furnace (Koyo KTF035N). The tube was purged with nitrogen purified by passing through a dehydrating and a deoxygenating column. The temperature of the tube furnace was increased at a rate of 10 °C min^{-1} to the desired temperature followed by cooling to ambient temperature under a flow of nitrogen (0.1 L min^{-1}).

Determination of iron content extracted by hydrochloric acid from Fe–C prepared by thermal treatment of 1.[42] Fe–C material prepared by thermal treatment of 1 at 500 °C (5.00 mg) was added to dilute hydrochloric acid (1 M, 2.0 mL) and water (5.0 mL) in a 25 mL measuring flask. The mixture was sonicated and left to stand for 3 h. Aqueous hydroxylamine hydrochloride solution (10 %, 1.0 mL), aqueous sodium acetate solution (30 %, 5.0 mL), and aqueous TPTZ solution (1 M, 1.0 mL) were added to the mixture. Water was added up to the gauge line of the measuring flask. A clear light blue solution was obtained after filtering off the carbon residue. The absorbance of the resulting solution at 595 nm was measured (Abs = 0.470). The absorbance of the blank sample at 595 nm was also measured (Abs = 0.052). The extracted iron content was calculated to be 2.6×10^{-2} mg.

Preparation of 3 on silica gel. Buckyruthenocene **3** (50.0 mg) was dissolved in CS_2. Silica gel (450 mg) was added to the CS_2 solution. The solvent was removed using a rotary evaporator, and then the resulting powder was dried under vacuum to obtain an orange-red powder. The ruthenium content was 0.90 % determined by XRF measurement using [$PdCl_2(PPh_3)_2$] as an internal standard.

Thermolysis of 3 on silica gel under a flow of nitrogen. The sample was placed in a quartz boat inside a quartz tube in a tube furnace (Koyo KTF035N). The tube was purged with nitrogen purified by passing through a dehydrating/deoxygenating column. The temperature of the tube furnace was increased at a rate of 10 °C min^{-1} to 500 °C, followed by cooling to ambient temperature under a flow of nitrogen (1.0 L min^{-1}).

Thermolysis of 3 on silica gel under a flow of hydrogen. Thermal treatment was carried out according to the above procedure except for using hydrogen (1.0 L min^{-1}). The ruthenium content was 0.78 % as determined by XRF measurement using [$PdCl_2(PPh_3)_2$] as an internal standard performed on SII SEA2120L fluorescence X-ray analyzer.

Catalytic hydrogenation of cyclohexene. The catalytic hydrogenation reaction was performed on an Endeavor system (Biotage). Ruthenium catalyst (0.50 μmol, 5 %-Ru/C (Aldrich, 1.05 mg), Ru-C/SiO_2-H_2 (0.78 % Ru, 6.47 mg)) was placed in a reaction vessel. The reaction apparatus was purged with hydrogen (1 bar). An ethanol solution of cyclohexene (2.0 M, 1 mL. 2 mmol) was added to the catalyst and additional ethanol (1.0 mL) was used to rinse the injection port. The reaction apparatus was heated to 50 °C, then hydrogen was pressurized to 10 bar and mechanical stirring was started. Hydrogen uptake was monitored with a computer-controlled data acquisition system.

Acknowledgements

The authors thank RIGAKU Corporation for the VT-XRD measurements. This research was partially supported by KAKENHI (18105004 and 1954017).

[1] *Metal Nanoparticles: Synthesis, Characterization, and Applications* (Eds: D. L. Feldheim, C. A. Foss, Jr.), Marcel Dekker, New York, **2002**.
[2] C. N. R. Rao, G. U. Kulkarni, P. J. Thomas, P. P. Edwards, *Chem. Soc. Rev.* **2000**, *29*, 27–35.
[3] M. Haruta, *Chem. Rec.* **2003**, *3*, 75–87.
[4] S. Eustis, M. A. El-Sayed, *Chem. Soc. Rev.* **2006**, *35*, 209–217.
[5] a) D. L. Leslie-Pelecky, R. D. Rieke, *Chem. Mater.* **1996**, *8*, 1770–1783; b) A.-H. Lu, E. L. Salabas, F. Schüth, *Angew. Chem.* **2007**, *119*, 1242–1266; *Angew. Chem. Int. Ed.* **2007**, *46*, 1222–1244.
[6] S. Yajima, M. Omori, *Nature* **1977**, *267*, 823–825.
[7] a) I. Lisiecki, M. P. Pileni, *J. Am. Chem. Soc.* **1993**, *115*, 3887–3896; b) D. Yin, S. Horiuchi, M. Morita, A. Takahara, *Langmuir* **2005**, *21*, 9352–9358.
[8] C. B. Murray, C. R. Kagan, M. G. Bawendi, *Annu. Rev. Mater. Sci.* **2000**, *30*, 545–610.
[9] Y.-P. Sun, H. W. Rollins, R. Guduru, *Chem. Mater.* **1999**, *11*, 7–9.
[10] a) K. S. Suslick, M. Fang, T. Hyeon, *J. Am. Chem. Soc.* **1996**, *118*, 11960–11961; b) K. S. Suslick, T. Hyeon, M. Fang, *Chem. Mater.* **1996**, *8*, 2172–2179; c) C. E. Bunker, J. J. Karnes, *J. Am. Chem. Soc.* **2004**, *126*, 10852–10853.
[11] a) K. Liu, S. B. Clendenning, L. Friebe, W. Y. Chan, X. B. Zhu, M. R. Freeman, G. C. Yang, C. M. Yip, D. Grozea, Z.-H. Lu, I. Manners, *Chem. Mater.* **2006**, *18*, 2591–2601; b) K. Liu, C.-L. Ho, S. Aouba, Y.-Q. Zhao, Z.-H. Lu, S. Petrov, N. Coombs, P. Dube, H. E. Ruda, W.-Y. Wong, I. Manners, *Angew. Chem.* **2008**, *120*, 1275–1279; *Angew. Chem. Int. Ed.* **2008**, *47*, 1255–1259.
[12] a) S. Miyanaga, H. Yasuda, A. Hiwara, A. Nakamura, H. Sakai, *J. Macromol. Sci. Part A: Pure Appl. Chem.* **1990**, *27*, 1347–1361; b) X. Chen, H. Song, *J. Mater. Sci.* **2007**, *42*, 8738–8744.
[13] a) E. Auer, A. Freund, J. Pietsch, T. Tacke, *Appl. Catal. A* **1998**, *173*, 259–271; b) B. F. G. Johnson, *Top. Catal.* **2003**, *24*, 147–159; c) C.-M. Ho, W.-Y. Yu, C.-M. Che, *Angew. Chem.* **2004**, *116*, 3365–3369; *Angew. Chem. Int. Ed.* **2004**, *43*, 3303–3307; d) M. K.-W. Choi, W.-

Y. Yu, M.-H. So, C.-Y. Zhou, Q.-H. Deng, C.-M. Che, *Chem. Asian J.* **2008**, *3*, 1256–1265.
[14] D. Astruc, F. Lu, J. R. Aranzaes, *Angew. Chem.* **2005**, *117*, 8062–8083; *Angew. Chem. Int. Ed.* **2005**, *44*, 7852–7872.
[15] a) Y. Motoyama, M. Takasaki, K. Higashi, S.-H. Yoon, I. Mochida, H. Nagashima, *Chem. Lett.* **2006**, *35*, 876–877; b) M. Takasaki, Y. Motoyama, K. Higashi, S.-H. Yoon, I. Mochida, H. Nagashima, *Chem. Asian J.* **2007**, *2*, 1524–1533.
[16] P. Serp, M. Corrias, P. Kalck, *Appl. Catal. A* **2003**, *253*, 337–358.
[17] B. Coq, J. M. Planeix, V. Brotons, *Appl. Catal. A* **1998**, *173*, 175–183.
[18] G. G. Wildgoose, C. E. Banks, R. G. Compton, *Small* **2006**, *2*, 182–193.
[19] a) A. Hashimoto, H. Yorimitsu, K. Ajima, K. Suenaga, H. Isobe, J. Miyawaki, M. Yudasaka, S. Iijima, E. Nakamura, *Proc. Natl. Acad. Sci. USA* **2004**, *101*, 8527–8530; b) J. Miyawaki, M. Yudasaka, H. Imai, H. Yorimitsu, H. Isobe, E. Nakamura, S. Iijima, *Adv. Mater.* **2006**, *18*, 1010–1014; c) J. Miyawaki, M. Yudasaka, H. Imai, H. Yorimitsu, H. Isobe, E. Nakamura, S. Iijima, *J. Phys. Chem. B* **2006**, *110*, 5179–5181.
[20] A. V. Talyzin, A. Dzwilewski, M. Pudelko, *Carbon* **2007**, *45*, 2564–2569.
[21] Y. Matsuo, E. Nakamura, *Chem. Rev.* **2008**, *108*, 3016–3028.
[22] a) M. Sawamura, Y. Kuninobu, E. Nakamura, *J. Am. Chem. Soc.* **2000**, *122*, 12407–12408; b) M. Sawamura, Y. Kuninobu, M. Toganoh, Y. Matsuo, M. Yamanaka, E. Nakamura, *J. Am. Chem. Soc.* **2002**, *124*, 9354–9355; c) M. Toganoh, Y. Matsuo, E. Nakamura, *Angew. Chem.* **2003**, *115*, 3654–3656; *Angew. Chem. Int. Ed.* **2003**, *42*, 3530–3532; d) M. Toganoh, Y. Matsuo, . E. Nakamura, *J. Am. Chem. Soc.* **2003**, *125*, 13974–13975; e) M. Toganoh, Y. Matsuo, E. Nakamura, *J. Organomet. Chem.* **2003**, *683*, 295–300; f) Y. Matsuo, E. Nakamura, *Organometallics* **2003**, *22*, 2554–2563; g) Y. Matsuo, Y. Kuninobu, S. Ito, E. Nakamura, *Chem. Lett.* **2004**, *33*, 68–69; h) Y. Kuninobu, Y. Matsuo, M. Toganoh, M. Sawamura, E. Nakamura, *Organometallics* **2004**, *23*, 3259–3266; i) Y. Matsuo, A. Iwashita, E. Nakamura, *Organometallics* **2005**, *24*, 89–95; j) Y. Matsuo, Y. Mitani, Y.-W. Zhong, E. Nakamura, *Organometallics* **2006**, *25*, 2826–2832; k) Y.-W. Zhong, Y. Matsuo, E. Nakamura, *Chem. Asian J.* **2007**, *2*, 358–366; l) Y. Matsuo, K. Matsuo, T. Nanao, R. Marczak, S. S. Gayathri, D. M. Guldi, E. Nakamura, *Chem. Asian J.* **2008**, *3*, 841–848.
[23] a) M. Sawamura, H. Iikura, E. Nakamura, *J. Am. Chem. Soc.* **1996**, *118*, 12850–12851; b) M. Sawamura, M. Toganoh, Y. Kuninobu, S. Kato, E. Nakamura, *Chem. Lett.* **2000**, *29*, 270–271; c) Y. Matsuo, A. Muramatsu, K. Tahara, M. Koide, E. Nakamura, *Org. Synth.* **2006**, *83*, 80–87.
[24] T. Kaji, T. Shimada, H. Inoue, Y. Kuninobu, Y. Matsuo, E. Nakamura, K. Saiki, *J. Phys. Chem. B* **2004**, *108*, 9914–9918.
[25] a) H. Nagashima, Y. Kato, H. Satoh, N. Kamegashima, K. Itoh, K. Oi, Y. Saito, *Chem. Lett.* **1996**, *25*, 519–520; b) N. Dragoe, K. Nakahara, L. Xiao, H. Shimotani, K. Kitazawa, *J. Therm. Anal. Calorim.* **1999**, *56*, 167–173.
[26] R. H. Herber, I. Nowik, Y. Matsuo, M. Toganoh, Y. Kuninobu, E. Nakamura, *Inorg. Chem.* **2005**, *44*, 5629–5635.
[27] H. S. Chen, A. R. Kortan, R. C. Haddon, D. A. Fleming, *J. Phys. Chem.* **1992**, *96*, 1016–1018.
[28] J. D. Crane, P. B. Hitchcock, H. W. Kroto, R. Taylor, D. R. M. Walton, *J. Chem. Soc. Chem. Commun.* **1992**, 1764–1765.
[29] a) Y. Saito, T. Yoshikawa, M. Okuda, N. Fujimoto, S. Yamamuro, K. Wakoh, K. Sumiyama, K. Suzuki, A. Kasuya, Y. Nishina, *Chem. Phys. Lett.* **1993**, *212*, 379–383; b) T. Hihara, H. Onodera, K. Sumiyama, K. Suzuki, A. Kasuya, Y. Nishina, Y. Saito, T. Yoshikawa, M. Okuda, *Jpn. J. Appl. Phys.* **1994**, *33*, L24L25.
[30] Z. Zhou, L. Ci, X. Chen, D. Tang, X. Yan, D. Liu, Y. Liang, H. Yuan, W. Zhou, G. Wang, S. Xie, *Carbon* **2003**, *41*, 337–342.
[31] a) T. Ichihashi, J. Fujita, M. Ishida, Y. Ochiai, *Phys. Rev. Lett.* **2004**, *92*, 215702; b) M. H. Rümmeli, F. Schäffel, C. Kramberger, T. Gemming, A. Bachmatiuk, R. J. Kalenczuk, B. Rellinghaus, B. Büchner, T. Pichler, *J. Am. Chem. Soc.* **2007**, *129*, 15772–15773.
[32] J. A. Moulijn, A. E. van Diepen, F. Kapteijn, *Appl. Catal. A* **2001**, *212*, 3–16.
[33] Z. M. Sheng, J. N. Wang, *Carbon* **2006**, *44*, 2096–2099.
[34] *Binary Alloy Phase Diagrams*, (Eds: T. B. Massalski, J. L. Murray, L. H. Bennett, H. Baker), American Society for Metals, Metals Park, Ohio, **1986**.
[35] D. M. Guldi, G. M. A. Rahman, R. Marczak, Y. Matsuo, M. Yamanaka, E. Nakamura, *J. Am. Chem. Soc.* **2006**, *128*, 9420–9427.
[36] CCDC 698570 contains the supplementary crystallographic data for this paper. These data can be obtained free of charge from The Cambridge Crystallographic Data Centre via www.ccdc.cam.ac.uk/data_request/cif.
[37] F. Su, F. Y. Lee, L. Lv, J. Liu, X. N. Tian, X. S. Zhao, *Adv. Funct. Mater.* **2007**, *17*, 1926–1931.
[38] a) Y. Matsuo, A. Muramatsu, Y. Kamikawa, T. Kato, E. Nakamura, *J. Am. Chem. Soc.* **2006**, *128*, 9586–9587; b) Y. Matsuo, K. Kanaizuka, K. Matsuo, Y.-W. Zhong, T. Nakae, E. Nakamura, *J. Am. Chem. Soc.* **2008**, *130*, 5016–5017.
[39] K. Hata, D. N. Futada, K. Mizuno, T. Namai, M. Yumura, S. Iijima, *Science* **2004**, *306*, 1362–1364.
[40] a) E. Nakamura, K. Tahara, Y. Matsuo, M. Sawamura, *J. Am. Chem. Soc.* **2003**, *125*, 2834–2835; b) Y. Matsuo, K. Tahara, M. Sawamura, E. Nakamura, *J. Am. Chem. Soc.* **2004**, *126*, 8725–8734; c) Y. Matsuo, K. Tahara, K. Morita, K. Matsuo, E. Nakamura, *Angew. Chem.* **2007**, *119*, 2902–2905; *Angew. Chem. Int. Ed.* **2007**, *46*, 2844–2847.
[41] J. N. Wang, L. Zhang, F. Yu, Z. M. Sheng, *J. Phys. Chem. B* **2007**, *111*, 2119–2124.
[42] a) P. F. Collins, H. Diehl, G. F. Smith, *Anal. Chem.* **1959**, *31*, 1862–1867; b) F. Nakashima, K. Sakai, *Bunseki Kagaku* **1962**, *11*, 73–77.

Received: August 26, 2008
Revised: October 20, 2008
Published online: January 9, 2009

